Synthesis and optical properties of cobalt-doped zinc aluminate nano pigments with an average crystallite size of 8 nm

M. Camacho-Espinoza
National Autonomous University of Mexico
A. Fernández-Osorio (ana8485@unam.mx)
National Autonomous University of Mexico
M. Tapia-Montalvo
National Autonomous University of Mexico
J. Chávez-Fernández
National Autonomous University of Mexico

Research Article

Keywords: ZnAl2O4, Cobalt ions, Spinel, Nano pigments

Posted Date: August 2nd, 2022

DOI: https://doi.org/10.21203/rs.3.rs-1889334/v1

Abstract

In this work, we report the synthesis of $Zn_{1-x}Co_xAl_2O_4$ x = 0, 0.01, 0.03, 0.06 nano pigments which were prepared by the coprecipitation method and heat treatment of precipitates. The samples were characterized using X-ray powder diffraction associated with the Rietveld refinement, UV-Vis spectroscopy, and transmission electron microscopy. The optical properties of the nano pigments, color development, crystal field strength, Racah parameters, and nephelauxetic parameters were investigated using spectroscopic data. The results show that sky blue ceramic nano pigments with normal spinel structure are obtained in samples annealed at 700°C for 2h, with an average crystallite size of 8 nm, with the incorporation of a very low concentration of Co^{2+} in the host lattice. The band gap of the nano pigments was calculated using Kubelka–Munk derived from the diffuse reflectance spectra. These nano pigments show high thermal stability and retain their blue color in the temperature range from 700 to 1300°C. Optical absorption spectra confirmed the substitution of zinc for cobalt in the $ZnAl_2O_4$ spinel, three absorption bands in the visible region and two intense bands are observed in the ultraviolet region. $Zn_{1-x}Co_xAl_2O_4$ x = 0, 0.01, 0.03, 0.06 nano pigments are insoluble in water, acids and bases. Results suggest that these nano pigments are candidates for use in cosmetics.

1. Introduction

Ceramic pigments are substances that develop color in inorganic solids and are capable of dispersing themselves at high processing temperatures without dissolution or chemical reaction. They are used in coatings for ceramic and glass, plastics, inks, paints, printing inks for paper and textiles, leather decoration, building materials, floor coverings, rubber, cosmetics, ceramic glazes, and enamels. The paint industry uses high-quality pigments where optimal, uniform particle size is important because it influences gloss, hiding power, tinting strength, and lightening power (Buxbaum and Pfaff 2005).

Color results from absorption and scattering phenomena across the visible region of the electromagnetic spectrum. Inorganic pigments often contain one or more transition metals, whose spectral absorptions are explained by crystal field d-d transitions. Nano pigments present a larger absorption area per mass colorant. Tinting strength increases as the particle size is reduced. Also, because of their high surface area, nano pigments ensure higher surface coverage (Cavalcante et al. 2009). Nano pigments with crystallite size less 10 nm present applications in cosmetics

automotive paints, wood finishes, artist colors, industrial coatings and some plastics.

$ZnAl_2O_4$ has the chemical formula of AB_2O_4 with a spinel structure. Spinel structures have cubic symmetry with a space group Fd3m and eight formula units per unit cell. In a normal spinel, the divalent A and tervalent B cations occupy tetrahedral and octahedral crystallographic sites, respectively (Sickafus et al. 2004). The spinel family develops a great variety of colors by doping with different chromophore ions and is probably the most used pigment structure. Spinels are resistant to attack and dissolution by chemical agents, including acids, bases, solvents, oxidizers, and reducing agents. Pigments with spinel

structure do not bleed in application and are heat stable to temperatures hundreds of degrees higher than organic pigments (O'Neill and Navrotsky 1983). They often absorb but are not discolored by UV light, making them good UV absorbers and opacifiers. They are lightfast, with no tendency to change color when exposed to hostile environments and are generally known and used for their weatherability (Smith 2002). Spinel pigments are inert materials since they do not contain soluble heavy metals. They are also insoluble in water, acids and bases.

The $Zn_{1-x}Co_xAl_2O_4$ system corresponds to a blue pigment in Group XIII of the CPMA classification (Color Pigments Manufacturers Association 2010). The optical band gap of polycrystalline $ZnAl_2O_4$ semiconductor is 3.8 eV, which indicates that zinc aluminate in the polycrystalline form is transparent for light with wavelengths > 320 nm. $ZnAl_2O_4$ is typically produced through high temperature (1000–1400°C) solid-state reactions in which metal oxide, or hydroxide, carbonate, or other raw materials capable of yielding oxides upon calcination, are intimately mixed and calcined in continuous or batch-style kilns (Yoneda et al. 2019). Solid-state reactions have been employed to make sub-micron spinel. Sol-gel, hydrothermal, and coprecipitation techniques have been employed to make nano-sized spinel (Zayat and Levy 2000; Chen et al. 2004; Andhare et al. 2020). In this work, we prepared Co^{2+}-doped zinc aluminate solid solutions using a simple coprecipitation method to obtain $Zn_{1-x}Co_xAl_2O_4$ powders with an average crystallite size of about 8 nm. Their optical properties were studied to evaluate their potential as candidates for cosmetic applications.

2. Experimental

2.1. Synthesis of samples

$ZnAl_{2-x}Cr_xO_4$, x = 0, 0.01, 0.03, and 0.06 nano pigments were prepared by a co-precipitation method and posterior heat treatment. The preparatory materials, zinc chloride, aluminum chloride, and cobalt chloride were provided by Merck company and used as received without further purification. Ammonium hydroxide was used as a precipitant agent. The precursors were mixed with deionized water in a glass beaker at room temperature to obtain a homogeneous solution. Then, a 30% NH_4OH solution was added dropwise until the white metal hydroxides precipitate appeared at pH 7.5. The resulting precipitate was washed twice with distilled water and oven-dried at 80°C for 6 h. Powders were placed in a high-alumina crucible and heated at 700°C for 2 h in the air to obtain $Zn_{1-x}Co_xAl_2O_4$ x = 0, 0.01, 0.03, and 0.06 nano pigments. The chemical reactions are:

$$ZnCl_2 + 2AlCl_3 \xrightarrow[NH_4OH]{H_2O} Zn(OH)_2 + 2Al(OH)_3 + 8NH_4Cl \xrightarrow[2h]{700\,^\circ C} ZnAl_2O_4 + 4H_2O$$

$$xCoCl_2 + (1\text{-}x)\ ZnCl_2 + 2AlCl_3 \xrightarrow[NH_4OH]{H_2O} xCo(OH)_2 + (1\text{-}x)\ Zn(OH)_2 + 2Al(OH)_3 + 8NH_4Cl \xrightarrow[2h]{700\,^\circ C} Zn_{(1-x)}Co_xAl_2O_4 + 4H_2O$$

2.2 Characterization

The X-ray diffraction pattern of the samples was recorded at room temperature with CuKa radiation in a Bruker Advance D-8 diffractometer. The structural refinements were performed by the Rietveld method with the Topas Academic software (Cohelo 2007)]. UV–visible electronic absorption spectra of the powdered samples were obtained by the diffuse reflectance technique with a Cary 5000 UV-Vis-NIR spectrophotometer. The values of crystal field strength (10Dq) and interelectronic repulsion Racah B parameter for Co^{2+} were determined from the energy levels of tetrahedral Co^{2+} ions in the Tanabe–Sugano d^3 diagram (d^7 ion in fourfold coordination). Colorimetric parameters, CIE-L*a*b* parameters were determined from the absorption spectra, employing illuminant D65 and 10º standard observer. Morphology of the nano pigments was observed using a JEOL FE-2010TEM analytical microscope operating at 200 kV by depositing a drop of the powdered nano pigments in ethanol onto 300-mesh Cu grids coated with a carbon layer.

All the measurements were performed on powdered samples at room temperature.

3. Results And Discussion

3.1. Phase and structures analysis

Figure 1 shows the XRD patterns of $Zn_{1-x}Co_xAl_2O_4$ (x = 0, 0.01, 0.03, 0.06) samples prepared by coprecipitation and heat treatment at 700°C for 2h.

The X-ray diffraction patterns of the samples are similar. The Co^{2+} ion concentration did not affect the crystalline structure of $ZnAl_2O_4$. All the synthesized nano pigments were single-phase samples containing only the spinel phase. In this system, Zn^{2+} ions occupied the tetrahedral sites, and Al^{3+} ions resided in the octahedral sites. Because Co^{2+} ions prefer the tetrahedral coordination (Ferguson et al. 1969), they will favor substitution on the tetrahedral Zn^{2+} site because of the similarity of crystal ionic radius. The ionic radii of Zn^{2+} and Co^{2+} ions in 4-fold coordination are 60 pm and 58 pm, respectively (Shannon and Prewitt 1969). Zn^{2+} and Co^{2+} also have identical charges, so no charge compensation is required before forming the substitutional solid solution. Co^{2+} in fourfold coordination is detectable at very low cobalt concentrations (Marfunin 1979), such as 1, 3 and 6 mol %, cobalt concentrations in these nano pigments.

The lattice parameters and crystallite size of these samples are obtained from the Rietveld refinements (Young and Wiles 1982; Coelho 2018). Figure 2 shows the XRD pattern of the $Zn_{0.99}Co_{0.01}Al_2O_4$ calcinated at 700°C for 2h.

Identification of the crystallographic phase was performed by indexing the X-ray powder diffraction pattern to Diffrac Suite EVA software (Bruker). The diffraction pattern showed the formation of a single phase with a spinel structure of $ZnAl_2O_4$ (gahnite). The positions and relative intensities of the observed XRD peaks are in good agreement with standard data of ICDD (2013), 01-077-9244 card, $ZnAl_2O_4$, which indicates the presence of the cubic lattice (FCC) with space group Fd3m.

3.2 Rietveld refinement

The powder XRD patterns of nano pigments for Rietveld refinement were collected at room temperature, and diffraction intensity was measured between 2θ ranges from 20–110°, with a 2θ step of 0.02° for 6.0 s per point. All the refined parameters, the crystallite size, lattice parameters, occupancy, fractional atomic positions, bond lengths, and bond angles calculated are listed in Table 1 for the $Zn_{0.99}Co_{0.01}Al_2O_4$, $Zn_{0.97}Co_{0.03}Al_2O_4$, and $Zn_{0.94}Co_{0.06}Al_2O_4$ samples annealed at 700°C for 2h. The refinement was started with the space group Fd3m, origin at 3m. The O^{2-} ions are located at the 32e, Zn^{2+} ions at the 8f, and Al^{3+} ions at the 16c Wyckoff position (Hahn 2006). In the first step, the global parameters and background were refined. In the next step, the structural parameters were refined. The typical refined XRD pattern of the samples is shown in Fig. 3.

The calculated pattern is the continuous line, and the lower curve is the weighted difference between the calculated and observed patterns. Vertical ticks mark the position of allowed reflections for the spinel phase present in the samples. The values of the discrepancy factor (R_{wp}) and the goodness of fit index ($\chi 2$) are listed in Table 1.

Table 1.

Parameters obtained from Rietveld refinements of $Zn_{1-x}Co_xAl_2O_4$ (x = 0, 0.01, 0.03, 0.06) samples obtained by a co-precipitation. Precipitates were annealed at 700°C for 2 h.

Parameters	Samples			
x Nominal cobalt content	0.00	0.01	0.03	0.06
Space group	Fd3m	Fd3m	Fd3m	Fd3m
Agreement factors:				
c2	1.97	2.10	2.00	2.22
R_{wp} (%)	6.37	7.18	7.24	7.92
Structural parameters:				
a (Å)	8.081	8.089	8.094	8.099
u	0.2531	0.2522	0.2521	0.2515
t	0	0	0	0
Crystallite size (nm)	7.875	7.694	7.611	7.536
Zn (ocupp.)	1	0.981	0.964	0.931
Co (occup.)	0	0.089	0.027	0.057
Al (occup.)	1	0.997	0.994	0.996
O (occup.)	1	0.991	0.989	0.988
Interatomic distances (Å)				
4-Coordinated polyhedron				
Zn – O(4)	1.953	1.956	1.955	1.954
4-Coordinated polyhedron				
Co – O(4)	1.968	1.967	1.968	1.967
6-Coordinated polyhedron				
Al – O(6)	1.900	1.910	1.910	1.930
Notes: *a* = lattice parameter; *u* = oxygen coordinate; t = inversion parameter				

The Rietveld refinement method was used to evaluate the effect of Co^{2+} ions on $ZnAl_2O_4$ crystals. The structural refinement results for $Zn_{1-x}Co_xAl_2O_4$ (x = 0, 0.01, 0.03, 0.06) crystals indicated that these crystals crystallized in a cubic structure (FCC) with space group Fd3m, and eight molecular formula per unit cell. It is a normal spinel. The value of the lattice constant was a = 8.081Å for x = 0, putting pure $ZnAl_2O_4$ in good agreement with the reported values (Wei and Chen 2006). In the doped samples the lattice parameter increases from 8.081 to 8.099 Å as increasing the cobalt concentration. Although the ionic radius of Co^{2+} is equal to 0.58 Å, which is smaller than the ionic radius of Zn^{2+} (i.e. 0.60 Å) a lattice

expansion takes place, due to a reduction of the covalence effect induced by the Co for Zn substitution (Ardit et al. 2012).

3.3 Transmission electron microscopy (TEM)

TEM was performed to determine particle morphology. TEM images of $Zn_{0.94}Co_{0.06}Al_2O_4$ are shown in Fig. 4. It revealed aggregates of nanoparticles in sphere-like form with crystallite sizes of about 9 nm. Average crystallite sizes determined by Rietveld refinement were 8.536 nm (Table 2), which are consistent with that obtained by the TEM technique.

3.4 Thermal stability

The XRD diffraction patterns of the $Zn_{1-x}Co_xAl_2O_4$ (x = 0.06) sample fired at different temperatures (700°C–1300°C) are illustrated in Fig. 5. A single spinel phase was obtained in all samples fired at 700–1200°C. The patterns showed characteristic spinel peaks. As the temperature increased, the crystallite size grew gradually, resulting in an increase in characteristic peak intensities and narrowing of the peak shapes. When the temperature increased to 1300°C, the intensity of all the spinel characteristic peaks was greatly enhanced, and the peak shapes were sharp, indicating that the crystallite size was increasing.

Studies have shown that the calcination temperature influences the growth rate of the crystal and the cation distribution in the spinel structure (Agarwal et al. 2016). X-ray diffraction analysis of the sample annealed at 1200°C shows the presence of a second phase, Al_2O_3, in addition to the spinel main phase, revealing the occurrence of a phase separation process due to the metastable character of the over-stoichiometric spinel. Al_2O_3 is present at 13% wt. according to the Rietveld refinement of the sample $Zn_{1-x}Co_xAl_2O_4$ (x = 0.06) fired at 1200°C for 2h (Fig. 6).

3.5 Band gap

The band gap was calculated to gain insight into the variation in optical properties of nanocrystalline zinc aluminate. The optical band gap was estimated from the diffuse reflectance spectra using the Tauc method and the Kubelka-Munk function (Tauc et al. 1966; López and Gómez 2012) with the equation:

$$\alpha = F(R) = \frac{(1-R)^2}{2R}$$

where, F (R) is the Kubelka-Munk function, α, the absorption coefficient, R, the reflectance. The Tauc relation:

$$F(R)\ h\nu = A\ (h\nu - E_g)^n$$

where $n = 1/2$ and 2 represents direct and indirect transitions. Extrapolation of linear regions of these plots to $(F(R)\ h\nu)^2 = 0$ gives the direct band gap values.

The plots of $(F(R)\ hv)^2$ versus hv for the $Zn_{1-x}Co_xAl_2O_4$ (x = 0, 0.01, 0.03, 0.06) samples annealed at 700°C for 2h are shown in Fig. 7.

The direct band gap value of the undoped $ZnAl_2O_4$ was observed to be 5.04 eV which is higher than the reported value of bulk zinc aluminate i.e., 3.8 eV (Sampath and Cordaro 1998), which can be attributed to the quantum confinement effect in zinc aluminate nanoparticles. Samples doped with cobalt, showed band gap goes on a slight decrease with increase in Co concentration, due to the difference in the electronic structure of the dopant. This band gap behavior has been observed in doped tin oxide nano particles (Ahmed et al. 2011). The calculated values of the energy of the gap band, cell parameter and average crystallite size obtained from Rietveld refinement are shown in Table 2.

Table 2

Cell parameter, average crystallite size and band gap of the $Zn_{1-x}Co_xAl_2O_4$ (x = 0.01, 0.03, 0.06) samples

Co concentration	Cell parameter	Average cryst. size	Band gap
X	(Å)	(nm)	(eV)
0.00	8.081	7.875	5.40
0.01	8.089	7.694	5.20
0.03	8.094	7.611	5.18
0.06	8.099	7.536	5.00

3.6 Optical properties

Optical properties were determined by UV-Vis absorption spectroscopy in powder samples. Figure 7 depicts the absorption spectra of the $Zn_{1-x}Co_xAl_2O_4$ (x = 0, 0.01, 0.03, 0.06) nano pigments annealed at 700°C for 2h. The optical spectra for Co^{2+} in the tetrahedral site exhibit three spin-allowed bands: $^4A_2 \rightarrow {}^4T_2\ (^4F)$, $^4A_2 \rightarrow {}^4T_1\ (^4F)$ and $^4A_2 \rightarrow {}^4T_1\ (^4P)$ (Duan et al. 2006). The first two fall in the infrared region, and only the third is present in the visible region, as a triple band around 590 nm.

$ZnAl_2O_4$ (x = 0) did not present absorption bands in the visible region, it is a white powder. The spectra were similar for the three samples with cobalt. Three absorption bands were observed centered at 546, 593, and 621 nm, corresponding to the electronic transition $^4A_2 \rightarrow {}^4T_1\ (^4P)$ of Co^{2+} in the tetrahedral coordination (Taran et al. 2009). The ground state was $^4A_2\ (^4F)$, the spin-allowed transitions occurred in quartet states ^4F and ^4P. The substitution of Co^{2+} for Zn^{2+} cations within the gahnite lattice can easily be observed in these spectra. The cobalt substitution was confirmed by a triplet of bands, which is characteristic of Co^{2+} ions in the tetrahedral sites (Ardit et al. 2014). These bands are assigned to the $^4A_2 \rightarrow {}^4T_1\ (^4P)$ transition, usually occurring as a triple band around 542 nm (green region), 584 nm (yellow-orange region), and 624 nm (red region) that results in the blue coloration of the samples. The triplet

bands are due to the significant effects of spin-orbital couplings, which split the 4T state into three spinner components (Izumi et al. 2007). The absorbance spectra show that the intensity of the triplet bands increases with an increase in cobalt concentration.

The color of the synthesized powders was investigated by colorimetric measurements and UV-Vis spectroscopy analysis. The CIE-L* a* b* colorimetric system (1977) is used to investigate the quantitative and qualitative characterizations of pigment and dye colors. The coordinates of a* and b* as two of the mutually orthogonal axes display the pigmentation or color dimensions. Lightness (L*) as the third axis is perpendicular to the a*, b* plane and has a value of 0 for black and 100 for white. Positive and negative a* values are attributed to red and green colors, respectively. Positive b* values are assigned to yellow color while negative values correspond to blue (Llusar et al. 2001).

The color parameters (L*, a*, b*) of the nano pigments calcined at 700°C for 2h are presented in Table 3.

Table 3

CIE-L*a*b* parameters of the $Zn_{1-x}Co_xAl_2O_4$ (x = 0.01, 0.03, 0.06) nano pigments (powders) annealed at 700°C for 2h.

Sample	L*	a*	b*
$Zn_{0.99}Co_{0.01}Al_2O_4$	88.6	-4.1	-15.1
$Zn_{0.97}Co_{0.03}Al_2O_4$	74.7	-3.8	-27.1
$Zn_{0.94}Co_{0.06}Al_2O_4$	69.9	-2.9	-29.8

The CIEL*a*b* parameters indicate the obtained nano pigment was situated in the blue-green field. The value of b* is highly negative, while the value of a* is only slightly negative, suggesting a blue color with a slightly green hue. The CIE values change with the variation of the pigment composition. The colorimetric parameters showed excellent blue shades in the powders. The parameter b*, responsible for the blue coloration, increased with cobalt concentration. Figure 9 presents the photographs of $Zn_{1-x}Co_xAl_2O_4$ (x = 0.01, 0.03, 0.06) samples prepared by coprecipitation and heat treatment in air at 700°C 2h.

The color of $ZnAl_2O_4$ is white, which elucidates the importance of Co^{2+} doping to control the color of the nano pigments.

3.7 Crystal field strength, Racah parameters, β-covalency values

The color change due to cobalt concentration can be related to the diminution of the crystal field parameter Δ_0 in the $Zn_{1-x}Co_xAl_2O_4$ solid solution. The influence of the host lattice on the Co^{2+} spectra was expressed by spectroscopic parameters such as the crystal field splitting (10Dq) and the B and C

Racah parameters (Burns 1993). The nephelauxetic is expressed by β. $\beta = B/B_0$, where B_0 is the Racah parameter of free ion value. The nephelauxetic effect is related to the covalency of Co^{2+} to ligand bonding, and a higher covalency reduces β (Lever and Rice 1969). The Co^{2+} ion has a d^7 electronic configuration and, in a tetrahedral crystal field, presents the splitting of the energy levels of a d^3 electronic configuration in an octahedral field, except for the value of the crystal field parameter Dq, which is smaller in the tetrahedral case (Dereń et al. 1994). The crystal field parameter 10Dq of 3d-ions depends on the mean metal-oxygen bond distances. In a point charge model, Δ_0 is linked to the M–O bond length, according to Eq. (1), (Brunold et al. 1996).

$$\Delta_0 = 10\ Dq = \frac{5}{3}\frac{qr^4}{R^5}$$

where q is the effective charge on ligands and r is the average radius of *d* orbitals. Here, both q and r can be assumed as constant for the same metal ion in the same ligand environment.

R is the mean metal-oxygen bond distance. In this case, R is the mean tetrahedral bond Co^{2+}- O^{2-} and Zn^{2+} - O^{2-} distance obtained from the Rietveld refinement. In the $ZnAl_2O_4$ spinel, Co^{2+} occupies a regular tetrahedron of T_d point symmetry with four equal M-O bond lengths varying ~ 1.968 Å according to the Rietveld refinement. The parameters were calculated and are collected in Table 4.

Table 4

Crystal field strength, Racah parameters and β-covalency of $Zn_{1-x}Co_xAl_2O_4$ (x = 0.01, 0.03, 0.06) nano pigments annealed at 700°C for 2h.

Parameter	$Zn_{0.99}Co_{0.01}Al_2O_4$	$Zn_{0.97}Co_{0.03}Al_2O_4$	$Zn_{0.94}Co_{0.06}Al_2O_4$
B (cm^{-1})	751	753	752
10Dq (cm^{-1})	4187	4156	4150
Dq/B	0.557	0.551	0.5518
b = B/Bo	0.7100	0.7119	0.7109

Changes in 10Dq were small, meaning the variation in the blue color in these pigments due to the increase in the concentration of Co^{2+} ion was minimal.

3.8 UV-Vis spectra at temperatures 700–1300°C

The absorption spectra of the $Zn_{0.97}Co_{0.03}Al_2O_4$ sample fired at different temperatures (700°C–1300°C) are shown in Fig. 10.

A triplet of bands appeared in the visible region at 550, 590, and 680 nm. These absorptions are ascribed to the $^4A_2 \rightarrow {}^4T_1$ (^4P) transition of Co^{2+} ions in tetrahedral symmetry, which gives a blue hue to the samples (Tanabe and Sugano 1956). The intensity of the bands increased with increasing temperature. Samples fired at 1200-1300°C are significantly stronger than those of other samples, meaning that these samples have a deeper blue hue. The nano pigments retain their blue color because the barycenter of the absorption band in spinel does not change with increasing temperature (Tangcharoen et al. 2019).

Table 5 presents the evolution of the values of the colorimetric parameters (L*, a*, and b*) of the $Zn_{0.97}Co_{0.03}Al_2O_4$ sample (powders) obtained at different temperatures. The annealing temperature had effects on the powder colorimetric parameters. In fact, the brightness of the powders increased with annealing temperature. The parameter -b*, responsible for the blue coloration, increased with temperature; meanwhile, the parameter -a*, responsible for green coloration, remained weak.

Table 5
CIE L* a* b* color parameters and observed color in $Zn_{0.97}Co_{0.03}Al_2O_4$ sample fired at different temperatures (700 – 1300°C)

T (°C)	Cryst. size (nm)	L*	a*	b*	Color
700	8.55	74.7	-3.8	-27.1	
900	10.23	70.2	0.5	-32.3	
1000	13.67	64.8	1.7	-42.2	
1100	22.83	58.3	1.4	-46.5	
1200	34.46	39.6	0.5	-47.5	
1300	45.14	35.2	0.3	-49.1	

Table 4 shows that the composition $x = 0.03$ obtained at annealing temperatures greater than 700°C exhibited higher values of the parameter b*. As the heat-treatment temperature increased, more Co^{2+} ions bonded to the tetrahedral sites in the $ZnAl_2O_4$ nanocrystals; therefore, the intensity of the absorption bands increased. The L* values decreased with temperature. The highest b* value was obtained at 1300°C. There was little variation in the blue color intensity with increasing temperature. We obtained blue powders using a low cobalt content (only 1, 3, and 6 mol%), representing a serious advantage of these nano pigments. The average crystallite size for the composition x = 0.03 (3 mol%) obtained at different temperatures was calculated using Scherrer's formula (B. E. Warren 1990) and the X-ray diffraction patterns of the samples. The absorption spectra of the $Zn_{0.94}Co_{0.03}Al_2O_4$ sample at temperatures 700-1300°C are presented in Fig.11.

Two intense bands are observed in the ultraviolet region (UV): a band centered at 251 nm assigned to absorption by the host lattice ($ZnAl_2O_4$) (Gaudon et al. 2009), and the band centered at 353 nm due to $O^{2-} \rightarrow Co^{2+}$ ligand-metal charge transition (LMCT) (Belyaev et al. 2019) in the visible region at 550, 590,

and 680 nm. These nano pigments have broad-spectrum sun protection, thereby improving protection against UVA and UVB. The capability to withstand the harmful effect of UV radiation increases with decrease in particle size. These nano pigments are potential candidates for cosmetic applications.

Conclusions

A blue spinel pigment with low cobalt content was obtained by coprecipitation from aqueous solutions and heat treatment of precipitates. Nano pigments were obtained at 700°C in single phase (gahnite) of $ZnAl_2O_4$ with an average crystallite size of about 8 nm. Rietveld refinement results showed that the as-synthesized $ZnAl_2O_4$:Co nano pigments exhibited normal spinel structure. $Zn_{1-x}Co_xAl_2O_4$ (x = 0.01, 0.03, 0.06) nano pigments are inert materials since they do not contain soluble heavy metals. They are also insoluble in water, acids and bases. These pigments showed high thermal stability and retained their blue color in the temperature range from 7*00 to 1300°C.* $ZnAl_2O_4$ band gap estimated using Kubelka–Munk derived from the diffuse reflectance spectroscopy measurements indicates a direct band gap of 5.04 eV, which can be attributed to the quantum confinement effect in zinc aluminate nanoparticles. The optical spectra were characterized by the occurrence of three absorption bands in the visible region corresponding to the electronic transition $^4A_2 \rightarrow {}^4T_1$ (^4P) of Co^{2+} in the tetrahedral coordination and two intense bands are observed in the ultraviolet region. These nano pigments are potential candidates for cosmetic applications.

Declarations

Acknowledgments

The support of this research by the UNAM-PAPIIT project IT100622 is gratefully acknowledged.

Author contributions The manuscript was written through the contributions of all authors. All authors have given approval to the final version of the manuscript

Conflict of interest The authors declare that there are no competing financial or non-financial interests that are directly or indirectly related to the work submitted for publication.

References

1. Agarwal H, Yadav TP, Srivastava ON, Shaz MA (2016) Cation distribution in nanocrystalline (Co, Ni)Al2O4 Spinel. Ceram Int. https://doi.org/10.1016/j.ceramint.2016.08.193
2. Ahmed AS, Shafeeq M. M, Singla ML, et al (2011) Band gap narrowing and fluorescence properties of nickel doped SnO 2 nanoparticles. J Lumin. https://doi.org/10.1016/j.jlumin.2010.07.017
3. Andhare DD, Patade SR, Kounsalye JS, Jadhav KM (2020) Effect of Zn doping on structural, magnetic and optical properties of cobalt ferrite nanoparticles synthesized via. Co-precipitation method. Phys B Condens Matter 583:412051. https://doi.org/10.1016/j.physb.2020.412051

4. Ardit M, Cruciani G, Dondi M (2012) Structural relaxation in tetrahedrally coordinated Co2+ along the gahnite-Co-aluminate spinel solid solution. Am Mineral. https://doi.org/10.2138/am.2012.4093
5. Ardit M, Dondi M, Cruciani G, Zanelli C (2014) Tetrahedrally coordinated Co2+in oxides and silicates: Effect of local environment on optical properties. Am Mineral 99:. https://doi.org/10.2138/am.2014.4877
6. B. E. Warren (1990) X-Ray Diffraction , New edition. Dover Publications Inc.
7. Belyaev A V., Lelet MI, Kirillova NI, et al (2019) Sol-gel synthesis and characterization of ZnAl2O4 powders for transparent ceramics. Ceram Int. https://doi.org/10.1016/j.ceramint.2018.11.179
8. Brunold TC, Güdel HU, Cavalli E (1996) Absorption and luminescence spectroscopy of Zn2SiO4 willemite crystals doped with Co2+. Chem Phys Lett. https://doi.org/10.1016/S0009-2614(96)00141-8
9. Burns RG (1993) Mineralogical applications of crystal field theory. Second edition. Mineral Appl Cryst F theory Second Ed
10. Buxbaum G, Pfaff G (2005) Industrial Inorganic Pigments. Wiley
11. Cavalcante PMT, Dondi M, Guarini G, et al (2009) Colour performance of ceramic nano-pigments. Dye Pigment 80:226–232. https://doi.org/10.1016/j.dyepig.2008.07.004
12. Chen Z-Z, Shi E-W, Li W-J, et al (2004) Preparation of nanosized cobalt aluminate powders by a hydrothermal method. Mater Sci Eng B 107:217–223. https://doi.org/10.1016/j.mseb.2003.11.013
13. Coelho AA (2018) TOPAS and TOPAS-Academic: An optimization program integrating computer algebra and crystallographic objects written in C++: An. J Appl Crystallogr. https://doi.org/10.1107/S1600576718000183
14. Cohelo A (2007) TOPAS-Academic, Coelho Software, Brisbane, Australia. Powder Diffr
15. Color Pigments Manufacturers Association (2010) CPMA Classification and Chemical Description of the Complex Inorganic Color Pigments, 4th ed. Alexandria
16. Dereń PJ, Str??k W, Oetliker U, Güdel HU (1994) Spectroscopic Properties of Co2+ Ions in MgAl2O4 Spinels. Phys status solidi 182:241–251. https://doi.org/10.1002/pssb.2221820125
17. Duan XL, Yuan DR, Wang LH, et al (2006) Synthesis and optical properties of Co2+-doped ZnGa2O4 nanocrystals. J Cryst Growth 296:. https://doi.org/10.1016/j.jcrysgro.2006.07.035
18. Ferguson J, Wood DL, Van Uitert LG (1969) Crystal-Field Spectra of d3,7 Ions. V. Tetrahedral Co 2+ in ZnAl 2 O 4 Spinel. J Chem Phys 51:2904–2910. https://doi.org/10.1063/1.1672431
19. Gaudon M, Apheceixborde A, Ménétrier M, et al (2009) Synthesis temperature effect on the structural features and optical absorption of Zn1-xCoxAl2O4 oxides. Inorg Chem. https://doi.org/10.1021/ic900482v
20. Hahn T (ed) (2006) International Tables for Crystallography. International Union of Crystallography, Chester, England
21. Izumi K, Miyazaki S, Yoshida S, et al (2007) Optical properties of 3d transition-metal-doped Mg Al2 O4 spinels. Phys Rev B - Condens Matter Mater Phys. https://doi.org/10.1103/PhysRevB.76.075111

22. Lever ABP, Rice SA (1969) Inorganic Electronic Spectroscopy. Phys Today. https://doi.org/10.1063/1.3035225
23. Llusar M, Forés A, Badenes JA, et al (2001) Colour analysis of some cobalt-based blue pigments. J Eur Ceram Soc. https://doi.org/10.1016/S0955-2219(00)00295-8
24. López R, Gómez R (2012) Band-gap energy estimation from diffuse reflectance measurements on sol-gel and commercial TiO 2: A comparative study. J Sol-Gel Sci Technol. https://doi.org/10.1007/s10971-011-2582-9
25. Marfunin AS (1979) Physics of Minerals and Inorganic Materials. Springer Berlin Heidelberg, Berlin, Heidelberg
26. O'Neill HSC, Navrotsky A (1983) Simple spinels: crystallographic parameters, cation radii, lattice energies, and cation distribution. Am Mineral
27. Sampath SK, Cordaro JF (1998) Optical properties of zinc aluminate, zinc gallate, and zinc aluminogallate spinels. J Am Ceram Soc. https://doi.org/10.1111/j.1151-2916.1998.tb02385.x
28. Shannon RD, Prewitt CT (1969) Effective ionic radii in oxides and fluorides. Acta Crystallogr Sect B Struct Crystallogr Cryst Chem 25:925–946. https://doi.org/10.1107/S0567740869003220
29. Sickafus KE, Wills JM, Grimes NW (2004) Structure of Spinel. J Am Ceram Soc 82:3279–3292. https://doi.org/10.1111/j.1151-2916.1999.tb02241.x
30. Smith HM (2002) High Performance Pigments - Wiley Online Library. Russell J Bertrand Russell Arch
31. Tanabe Y, Sugano S (1956) On the Absorption Spectra of Complex Ions, III the Calculation of the Crystalline Field Strength. J Phys Soc Japan. https://doi.org/10.1143/JPSJ.11.864
32. Tangcharoen T, T-Thienprasert J, Kongmark C (2019) Effect of calcination temperature on structural and optical properties of MAl2O4 (M = Ni, Cu, Zn) aluminate spinel nanoparticles. J Adv Ceram. https://doi.org/10.1007/s40145-019-0317-5
33. Taran MN, Koch-Müller M, Feenstra A (2009) Optical spectroscopic study of tetrahedrally coordinated Co2+ in natural spinel and staurolite at different temperatures and pressures. Am Mineral 94:. https://doi.org/10.2138/am.2009.3247
34. Tauc J, Grigorovici R, Vancu A (1966) Optical Properties and Electronic Structure of Amorphous Germanium. Phys status solidi. https://doi.org/10.1002/pssb.19660150224
35. Wei X, Chen D (2006) Synthesis and characterization of nanosized zinc aluminate spinel by sol-gel technique. Mater Lett. https://doi.org/10.1016/j.matlet.2005.10.024
36. Yoneda M, Gotoh K, Nakanishi M, et al (2019) Solid-state synthesis and characterization of cobalt blue core-shell pigment particles. J Am Ceram Soc 102:3468–3476. https://doi.org/10.1111/jace.16191
37. Young RA, Wiles DB (1982) Profile shape functions in Rietveld refinements. J Appl Crystallogr 15:430–438. https://doi.org/10.1107/S002188988201231X
38. Zayat M, Levy D (2000) Blue CoAl 2 O 4 Particles Prepared by the Sol–Gel and Citrate–Gel Methods. Chem Mater 12:2763–2769. https://doi.org/10.1021/cm001061z

39. (2013) International Centre for Diffraction Data. Micros Today 21:8–8. https://doi.org/10.1017/S1551929513000254
40. (1977) CIE Recommendations on Uniform Color Spaces, Color-Difference Equations, and Metric Color Terms. Color Res Appl 2:5–6. https://doi.org/10.1002/j.1520-6378.1977.tb00102.x

Figures

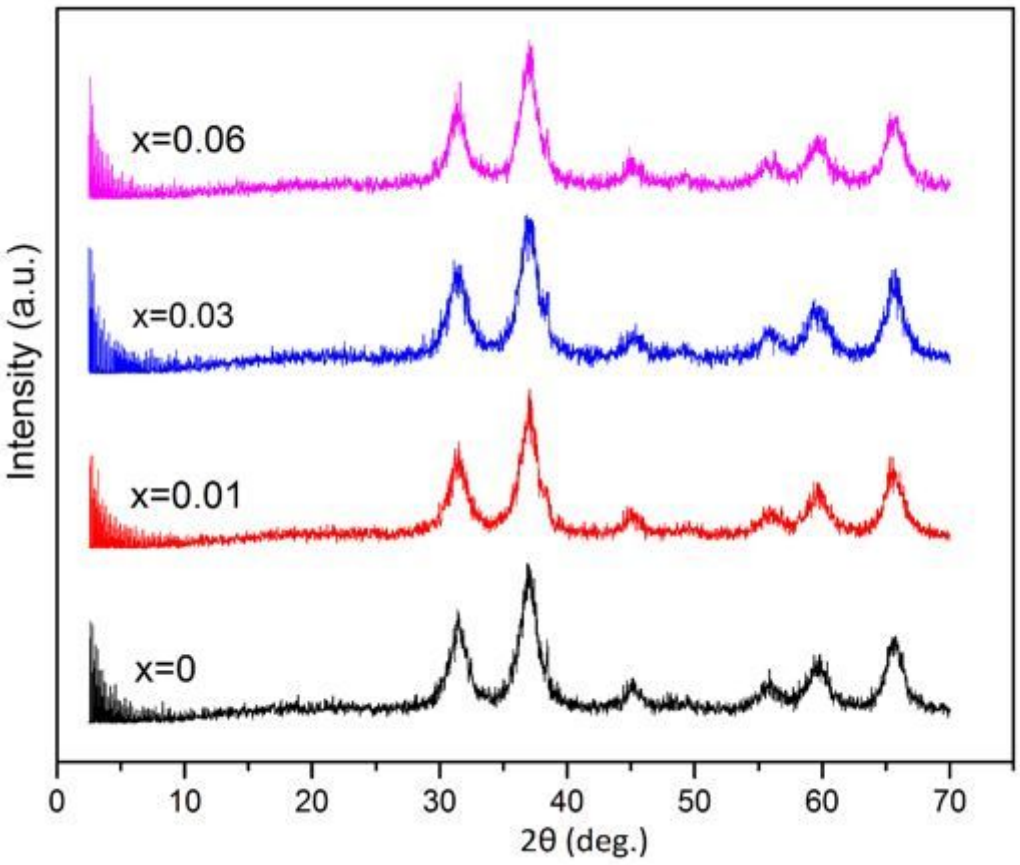

Figure 1

XRD patterns of $Zn_{1-x}Co_xAl_2O_4$ (x =0, 0.01, 0.03, 0.06) samples prepared by a coprecipitation and heat treatment at 700°C for 2h

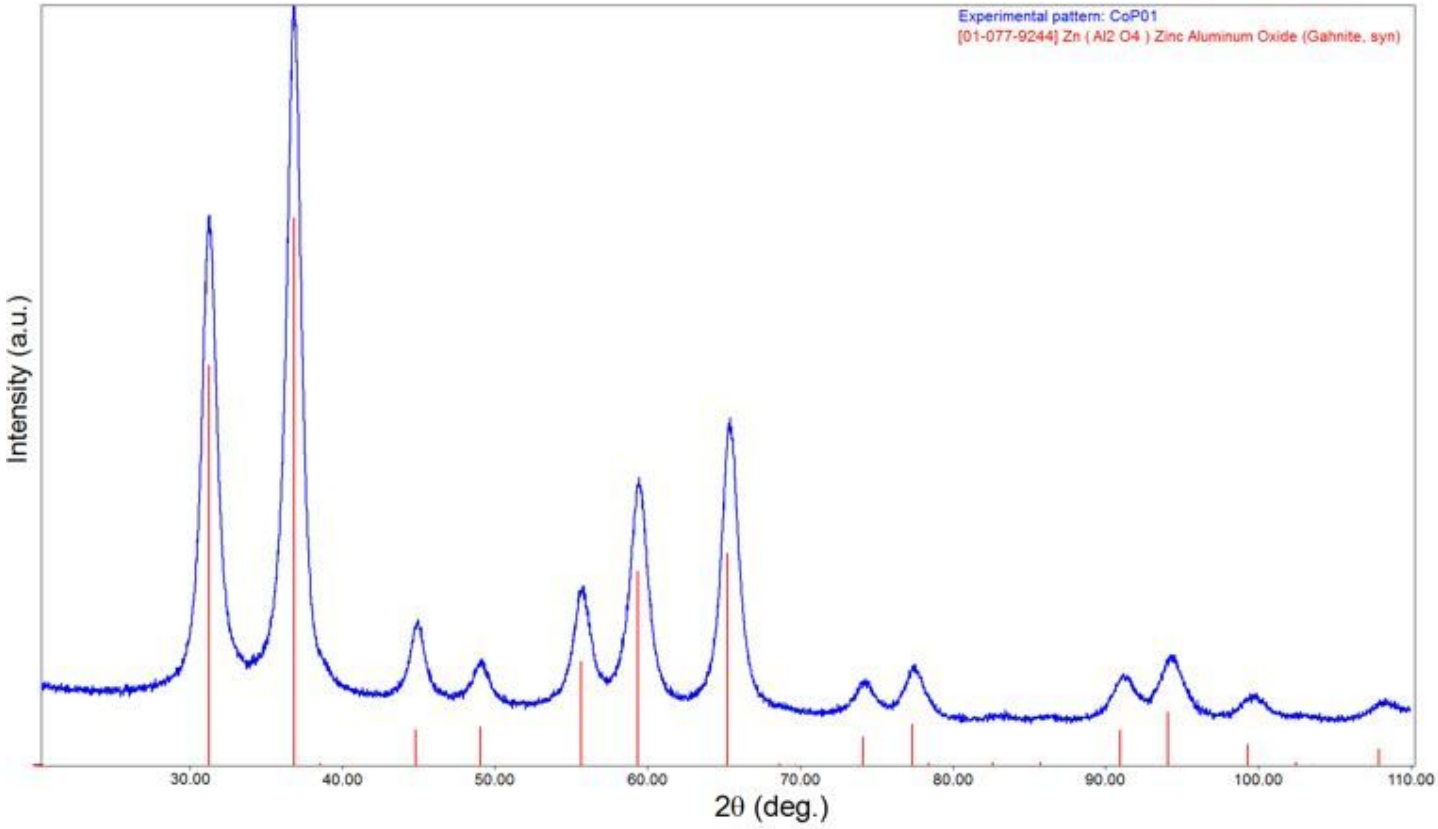

Figure 2

XRD pattern of the $Zn_{0.99}Co_{0.01}Al_2O_4$ sample

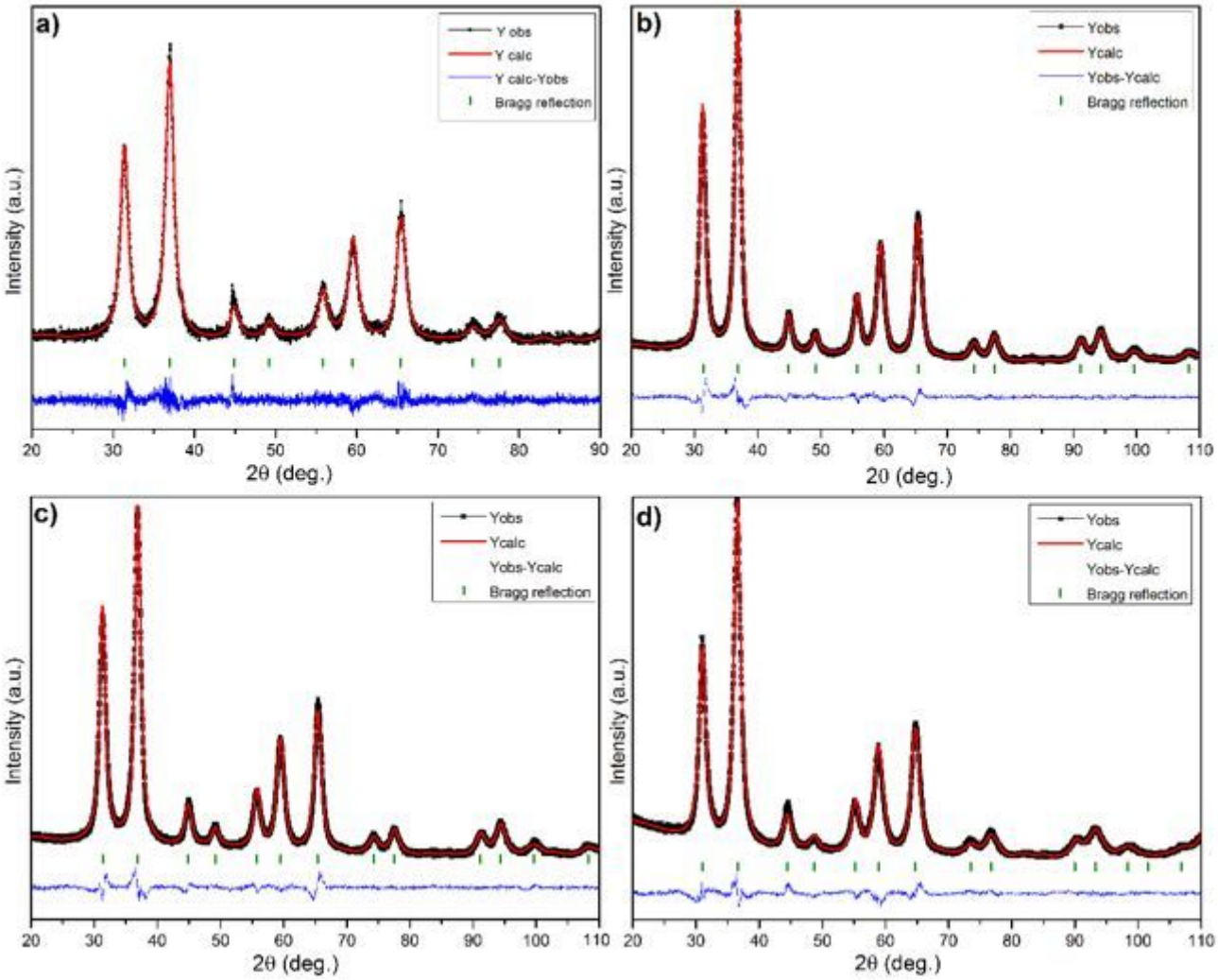

Figure 3

Plot of Rietveld refinements performed on X-ray powder diffraction data of (a) $ZnAl_2O_4$ (b) $Zn_{0.99}Co_{0.01}Al_2O_4$ (c) $Zn_{0.97}Co_{0.03}Al_2O_4$ (d) $Zn_{0.94}Co_{0.06}Al_2O_4$

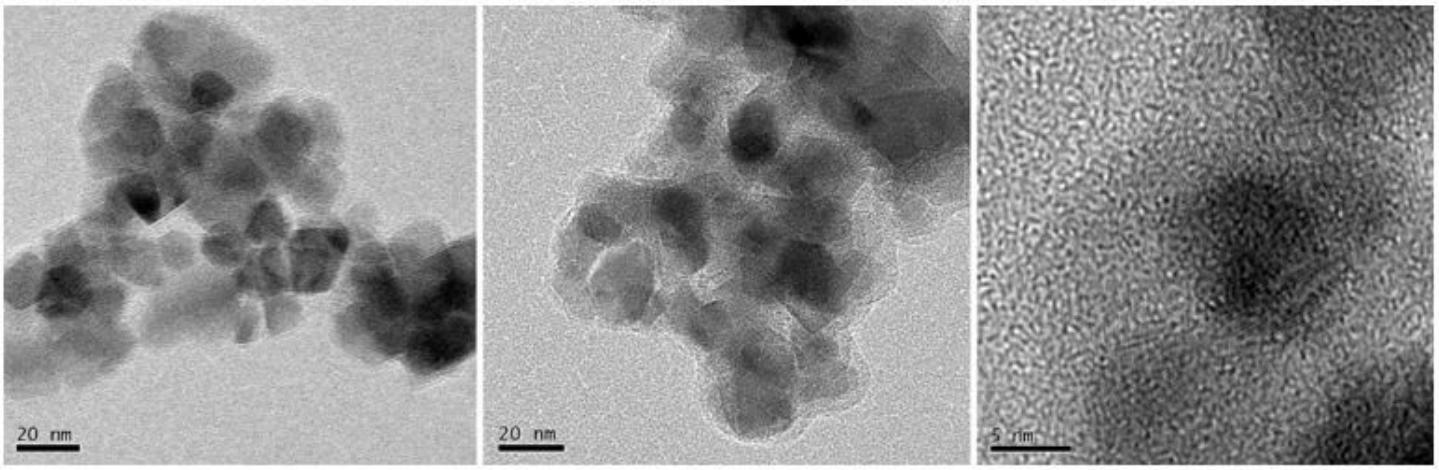

Figure 4

TEM images of $Zn_{0.94}Co_{0.06}Al_2O_4$ sample prepared by coprecipitation and heat treatment in air at 700°C 2h

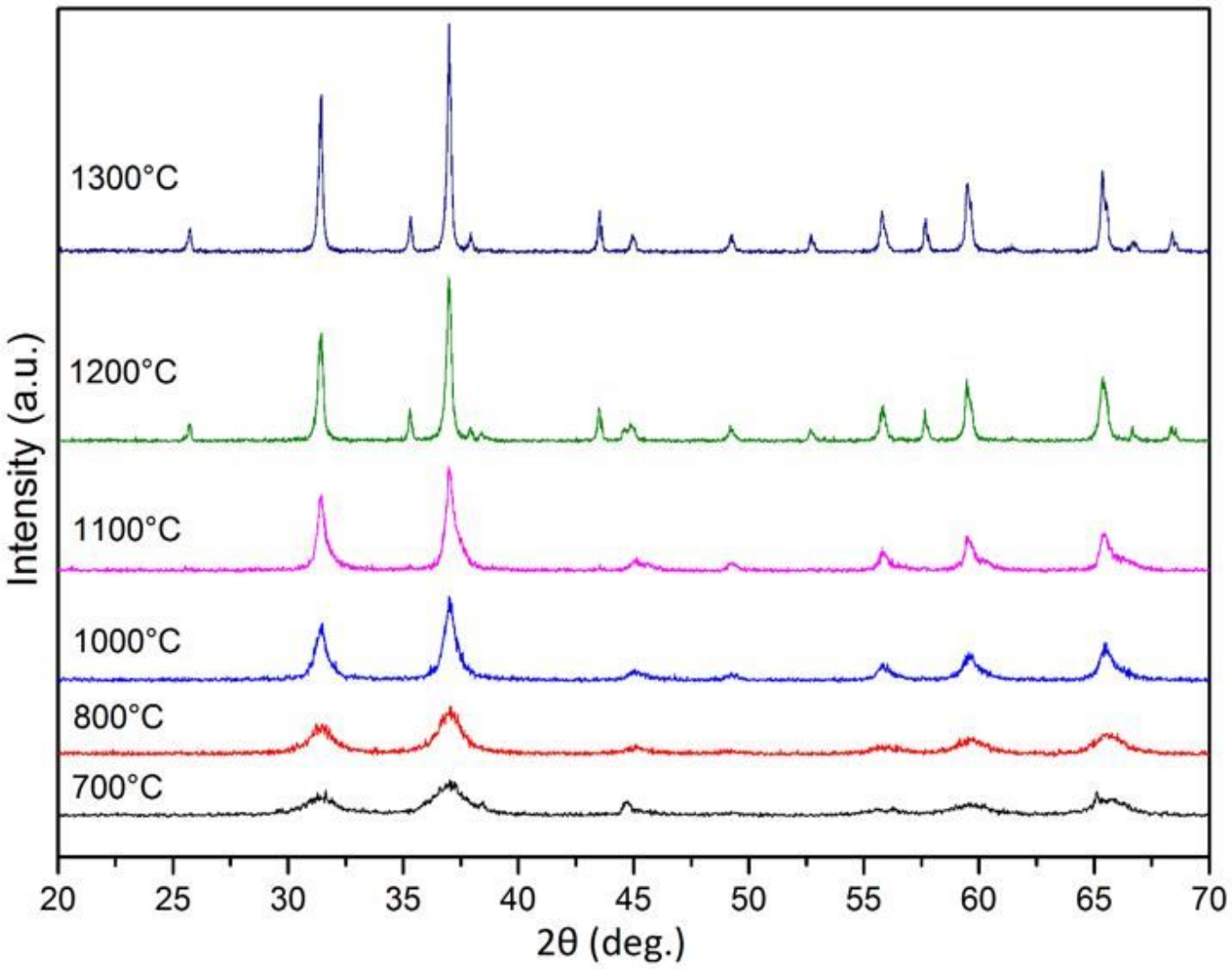

Figure 5

XRD diffraction patterns of the $Zn_{1-x}Co_xAl_2O_4$ (x = 0.06) sample fired at different temperature

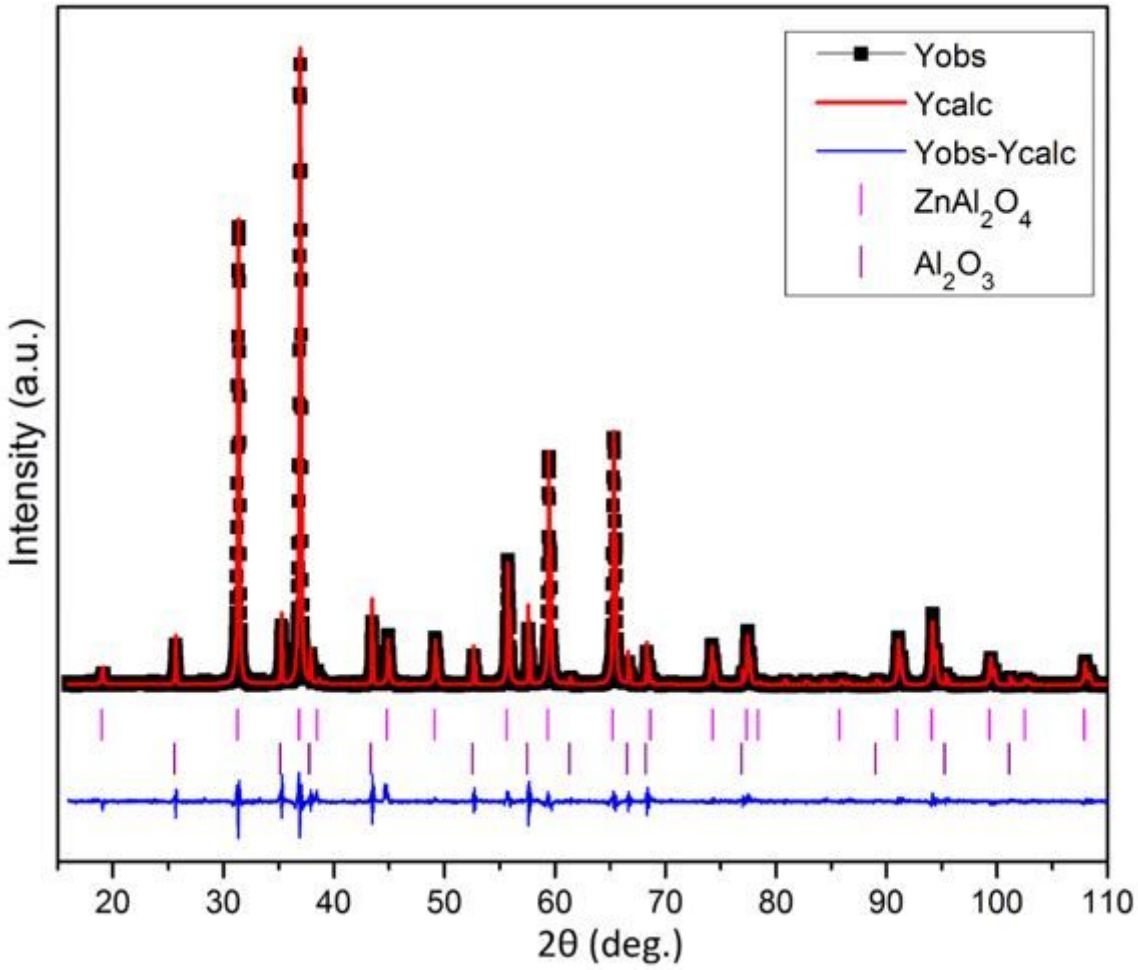

Figure 6

Rietveld refinement of the sample $Zn_{1-x}Co_xAl_2O_4$ (x = 0.06) fired at 1200°C for 2h

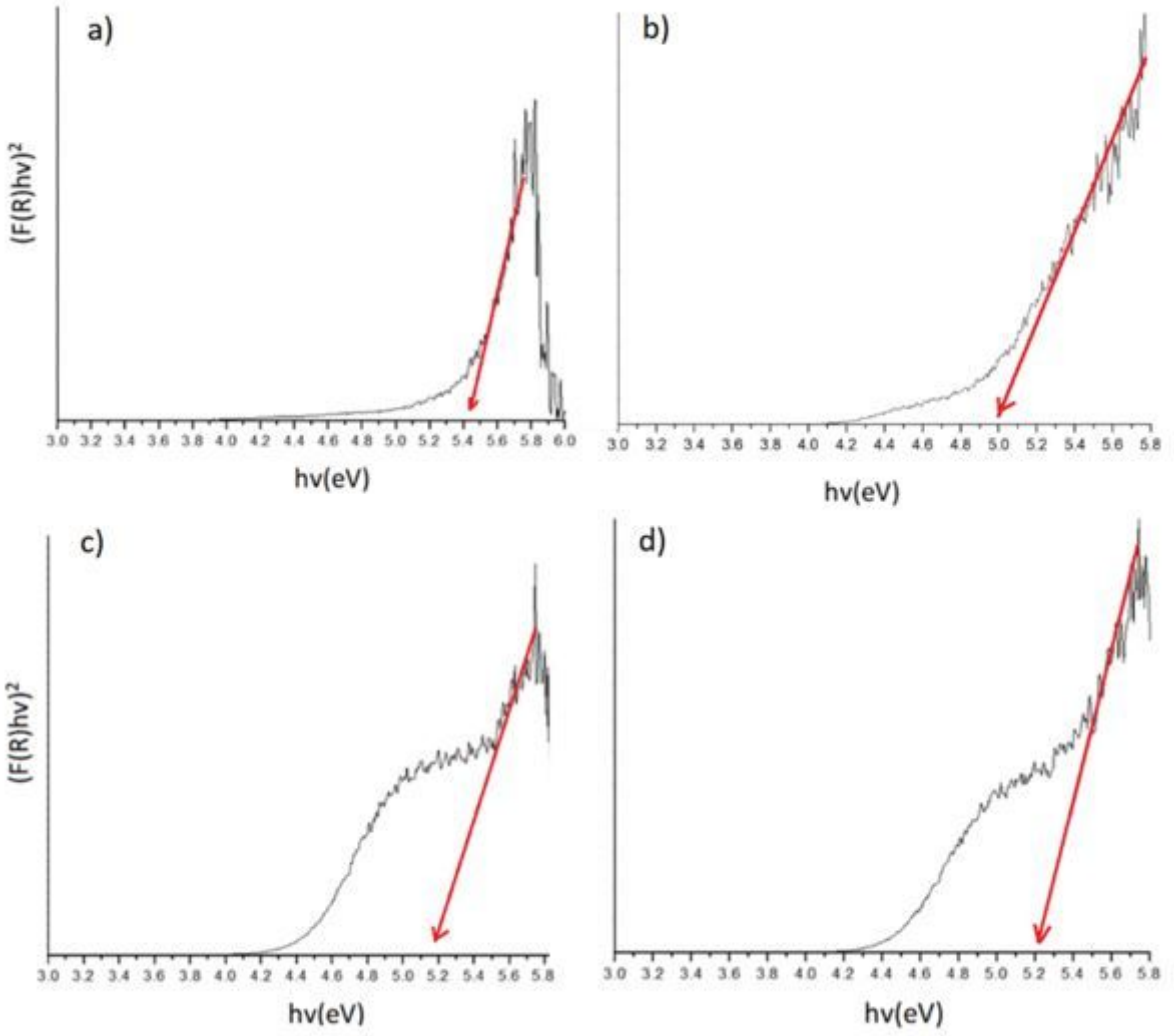

Figure 7

Plot of $(F(R)\ hn)^2$ versus hn for $Zn_{1-x}Co_xAl_2O_4$ (x = 0.01, 0.03, 0.06) samples (a) $ZnAl_2O_4$ (b) $Zn_{0.99}Co_{0.01}Al_2O_4$ (c) $Zn_{0.97}Co_{0.03}Al_2O_4$ (d) $Zn_{0.94}Co_{0.06}Al_2O_4$

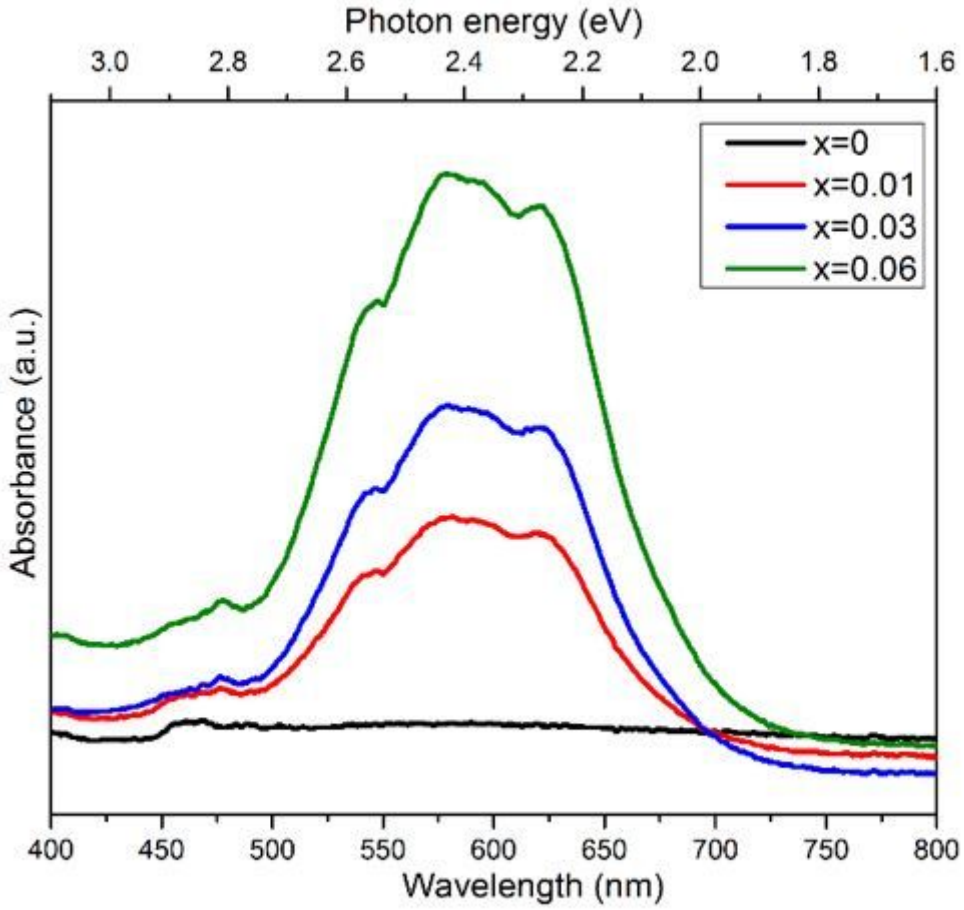

Figure 8

Absorption spectra of the $Zn_{1-x}Co_xAl_2O_4$ (x = 0, 0.01, 0.03, 0.06) nano pigments annealed at 700°C for 2h

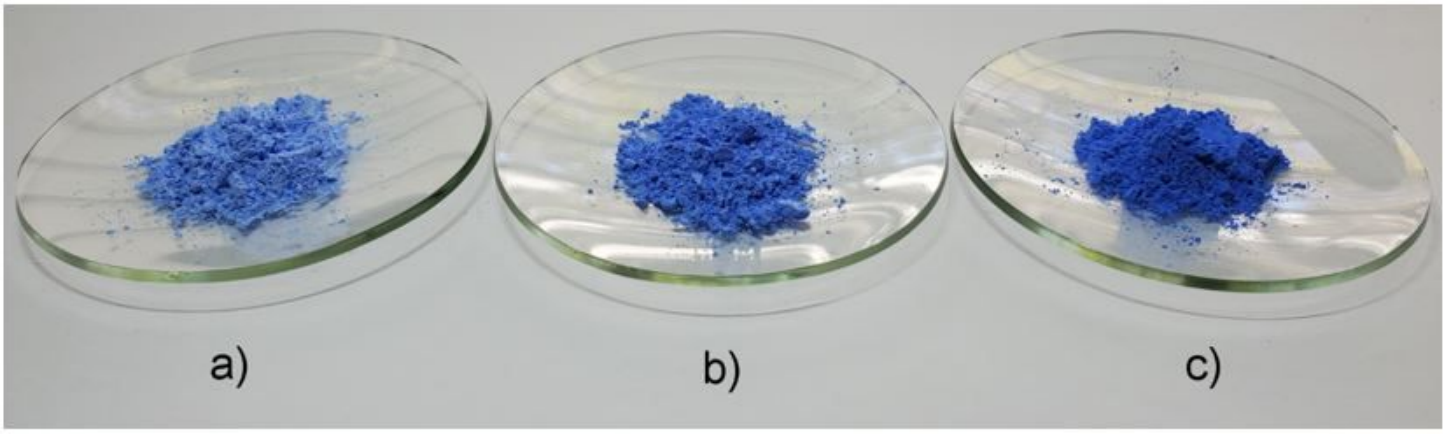

Figure 9

Representative photographs of the samples: (a) $Zn_{0.99}Co_{0.01}Al_2O_4$, (b) $Zn_{0.97}Co_{0.03}Al_2O_4$ and (c) $Zn_{0.94}Co_{0.06}Al_2O_4$; annealed at 700°C for 2h

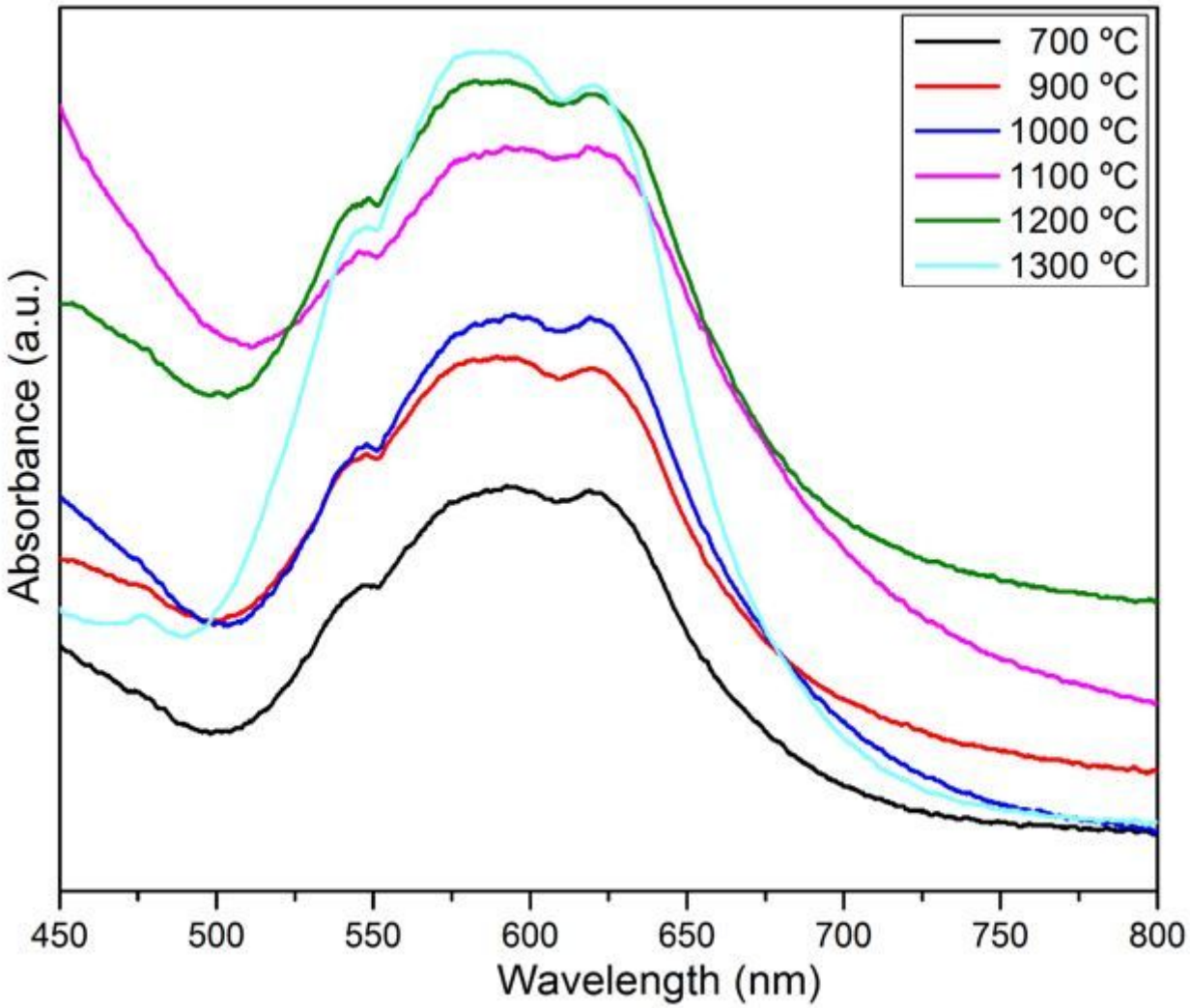

Figure 10

Absorption spectra of the $Zn_{0.97}Co_{0.03}Al_2O_4$ sample fired at different temperatures

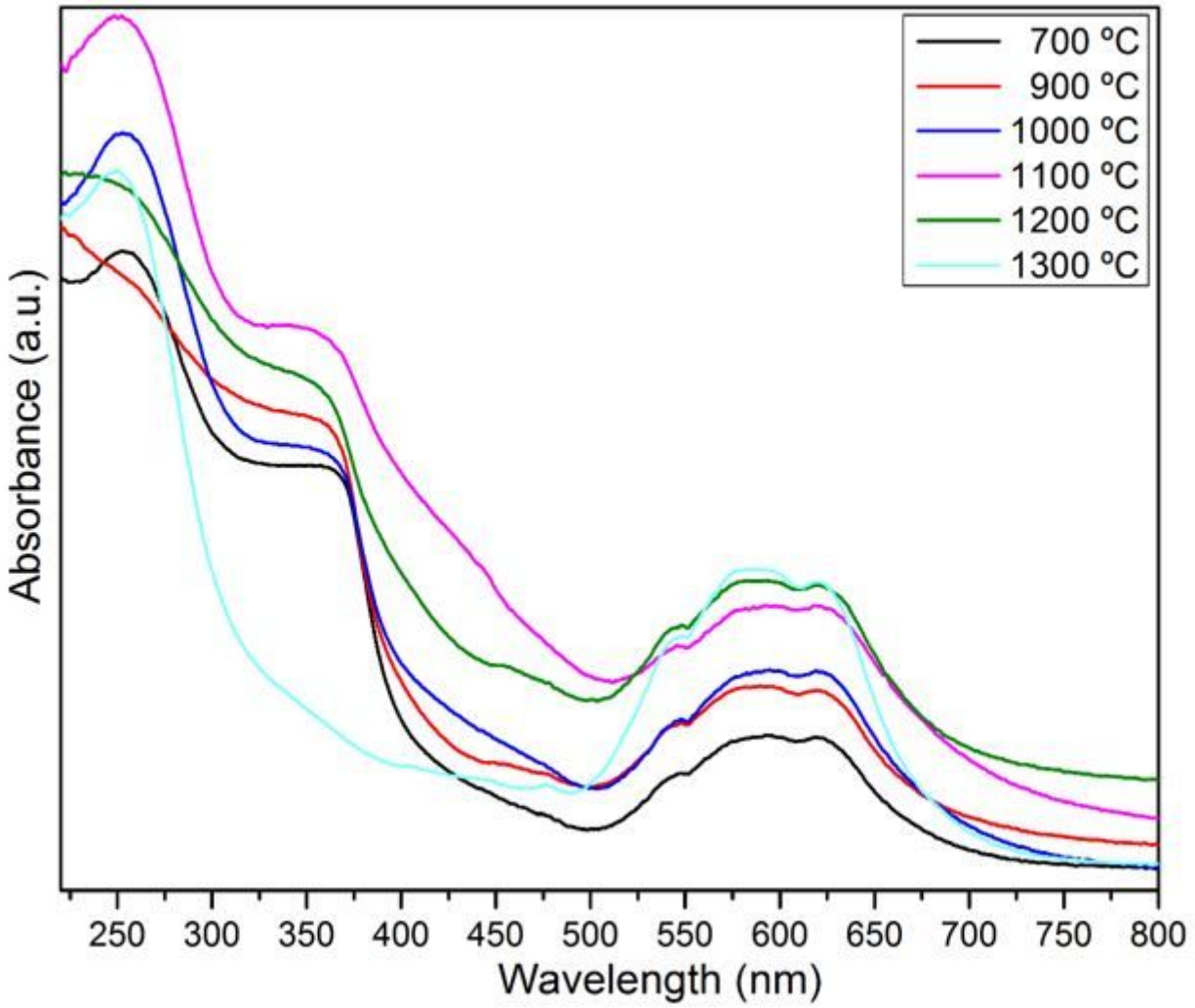

Figure 11

UV-Vis absorption spectra of the $Zn_{0.94}Co_{0.06}Al_2O_4$ sample fired at different temperatures